Newton

Article

Macroscale anomalous heat conduction in active thermal metamaterials

Graphical abstract

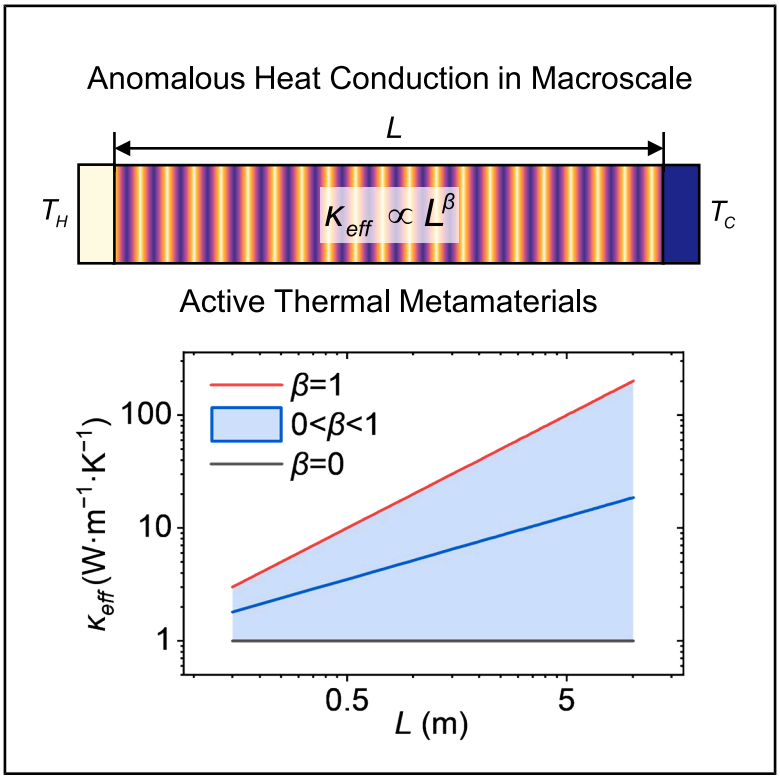

Highlights

- First demonstration of macroscale anomalous heat conduction provided
- Size-dependent effective thermal conductivity $\kappa_{eff} \propto L^{\beta}$ with β from 0 to 1 revealed

Authors

Zhaochen Wang, Quan Liu, Linyi Xiang, ..., Xin Qian, Xiaobing Luo, Run Hu

Correspondence

hurun@hust.edu.cn

In brief

Anomalous heat conduction, a non-Fourier phenomenon characterized by size-dependent effective thermal conductivity, was previously thought to be limited to the microscale. Wang et al. overcome this scale limitation and achieve macroscale anomalous heat conduction via active thermal metamaterials, demonstrating size-dependent effective thermal conductivity as $\kappa_{eff} \propto L^{\beta}$. The exponent β ranges from 0 to 1, controlled by modulating heat/cold sources. These results provide new insights into anomalous heat conduction and advanced thermal functionalities.

Wang et al., 2025, Newton *1*, 100255
November 3, 2025
https://doi.org/10.1016/j.newton.2025.100255

CellPress

Please cite this article in press as: Wang et al., Macroscale anomalous heat conduction in active thermal metamaterials, Newton (2025), https://doi.org/10.1016/j.newton.2025.100255

Newton

CellPress
OPEN ACCESS

Article

Macroscale anomalous heat conduction in active thermal metamaterials

Zhaochen Wang,[1] Quan Liu,[1] Linyi Xiang,[1] Zhiqiang Wang,[2] Wubin Kong,[2] Yonggang Yao,[3] Xin Qian,[1] Xiaobing Luo,[1] and Run Hu[1,4,5,6,*]

[1]School of Energy and Power Engineering, Huazhong University of Science and Technology, Wuhan 430074, China
[2]School of Electrical and Electronic Engineering, Huazhong University of Science and Technology, Wuhan 430074, China
[3]School of Materials Science and Engineering, Huazhong University of Science and Technology, Wuhan 430074, China
[4]Department of Applied Physics, Kyung Hee University, 1732 Deogyeong-daero, Giheung-gu, Yongin-Si, Gyeonggi-do 17104, Republic of Korea
[5]Shenzhen Institute of Huazhong University of Science and Technology, Shenzhen 518052, China
[6]Lead contact
*Correspondence: hurun@hust.edu.cn
https://doi.org/10.1016/j.newton.2025.100255

ACCESSIBLE OVERVIEW In macroscale systems, heat conduction typically follows Fourier's law, with thermal conductivity independent of size. However, at the microscale, this behavior can break down: when system dimensions approach the mean free path of heat carriers, heat conduction becomes "anomalous," characterized by an effective thermal conductivity κ_{eff} that diverges with system size l as $\kappa_{eff} \propto l^{\beta}$. The exponent β delineates different regimes: diffusive ($\beta = 0$), ballistic-diffusive ($0 < \beta < 1$), and ballistic ($\beta = 1$). While such phenomena have mainly been observed at the microscale, this work presents the macroscale counterpart through active thermal metamaterials (ATMs)—structures embedded with programmable heat and cold sources. By strategically arranging these sources within a base material, ATMs reconfigure internal temperature fields to mimic microscale anomalies, enabling the extraction of size-dependent κ_{eff} as $\kappa_{eff} \propto L^{\beta}$ at the macroscale, with β spanning from 0 to 1—an unreported observation in anomalous heat conduction. Both simulations and experiments validate this sense-breaking phenomenon, supported by detailed physics discussions. The size-dependent κ_{eff} allows for tailoring materials by modulating heating, cooling, or system size. These reconfigurable ATMs can be dynamically adjusted to create thermal functional devices with arbitrary shapes, dimensions, and even functionalities, opening new avenues for advancing thermal management and innovative thermal metamaterials.

SUMMARY

Anomalous heat conduction is a non-Fourier phenomenon that typically occurs at the microscale, where the mean free path of thermal carriers approaches the system size, but its macroscale counterpart has been lacking. Here, we introduce the concept of active thermal metamaterials (ATMs) based on internal source modulation, demonstrating a macroscopic analog to microscale anomalous heat conduction with size-dependent effective thermal conductivity, $\kappa_{eff} \propto L^{\beta}$. The tunable exponent β from 0 to 1 allows for mimicking various microscale anomalous heat conduction phenomena. This approach can potentially ease the design of desired-κ materials by adjusting system size, significantly expanding the capability realm of thermal metamaterials and opening new avenues for advanced thermal management and functionalities.

INTRODUCTION

Anomalous heat conduction, as pioneered by Fermi, Pasta, and Ulam (FPU) in the context of one-dimensional (1D) nonlinear dynamics and system thermalization,[1] has garnered interest due to its rich physics and potential to violate classical Fourier's law. Since then, it has been observed in various low-dimensional systems, including nanowires,[2,3] molecular chains,[4,5] nanotubes,[6,7] nanofibers,[8,9] nonlinear lattices,[10–12] and even 1D fluids.[13] In such systems, the effective thermal conductivity κ_{eff} typically scales with system size l, as $\kappa_{eff} \propto l^{\beta}$, with different regimes: diffusive ($\beta = 0$), ballistic-diffusive ($0 < \beta < 1$), and ballistic ($\beta = 1$) (Figure 1A). Macroscale heat conduction is mostly diffusive, described by Fourier's law, as κ is a size-independent constant ($\beta = 0$) (Figure 1B), while in the microscale, anomalous phenomena such as size effect,[14] ballistic/diffusive crossover,[15–17]

Please cite this article in press as: Wang et al., Macroscale anomalous heat conduction in active thermal metamaterials, Newton (2025), https://doi.org/10.1016/j.newton.2025.100255

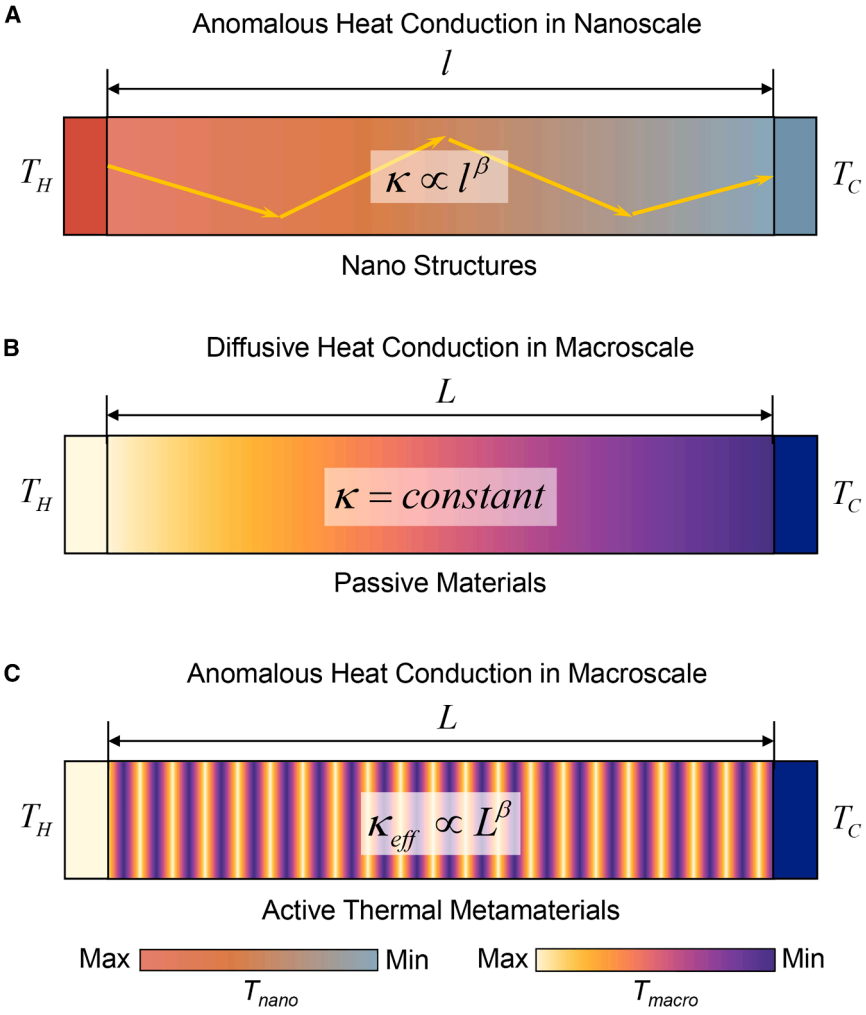

Figure 1. Origin of anomalous heat conduction

(A) Anomalous heat conduction in nanoscale. The effective thermal conductivity κ_{eff} typically scales with nanoscale system size l, as $\kappa_{eff} \propto l^{\beta}$ in nanostructures.

(B) Diffusive heat conduction in macroscale. Macroscale heat conduction in passive materials is mostly diffusive, described by Fourier's law, as κ is a size-independent constant. L represents the system size in macroscale.

(C) Anomalous heat conduction in macroscale with ATMs. ATMs incorporate spatially embedded heat sources with adjustable thermal powers, enabling size-dependent κ_{eff} as $\kappa_{eff} \propto L^{\beta}$ and an oscillating temperature field.

second sound,[18] hydrodynamic phonon transport,[19] Anderson phonon localization,[20] quantized heat conduction,[21] and coherent heat transport[22] offer diverse possibilities for microscale thermal management and energy conversion. It remains an open question whether these mechanisms can be extended to the macroscale or if the anomalous size-dependent κ_{eff} can be realized at larger scales.

Thermal metamaterials have revolutionized traditional thermal management by enabling unprecedented control over heat flow, leading to some eye-catching functionalities and phenomena[23–28] such as cloaking[29–31] and concentrating.[32–34] Their core principle is the precise regulation of the anisotropic thermal conductivity tensor, derived from space transformations in transformation thermotics, i.e., $\kappa = \frac{J'\kappa_0 J}{\det(J)}$ where J is the Jacobian matrix of the space transformation as $J = \frac{\partial x'}{\partial x}$, with x as the general coordinate. Typically, fabrication uses multi-layered or drilled structures combining high-κ material (usually copper) and low-κ material (e.g., air or polydimethylsiloxane [PDMS]) to approximate the anisotropic thermal conductivity tensors after some empirical design or numerical optimization, such as genetic algorithms and topological optimization.[32,35] However, the upper limit of κ_{eff} is determined by the high-κ component, constraining the capability and flexibility of thermal metamaterials. Recent advances with passive or active methods,[36–38] such as spinning water,[39] extended plane,[40] and thermal dipole,[41] aim to overcome this but are limited by spatial and shape constraints. Achieving size-dependent κ_{eff} would allow real-time, adjustable thermal conductivity exceeding that of common materials, such as copper with 400 $W \cdot m^{-1} \cdot K^{-1}$, greatly expanding the design space for thermal metamaterials.

In this paper, we present a strategy to realize macroscale anomalous heat conduction via active thermal metamaterials (ATMs). Unlike conventional thermal metamaterials, ATMs incorporate spatially embedded heat sources with adjustable thermal powers, enabling size-dependent κ_{eff} and surpassing the properties of natural materials. We demonstrate phenomena beyond the diffusive regime, mimicking ballistic and ballistic-diffusive heat conduction (Figure 1C). As a proof of concept, we achieve anomalous temperature profiles and obtain κ_{eff} values exceeding those of copper.

RESULTS

ATM model

The ATM is composed of a base medium and multiple controllable internal heat sources. The base medium is a natural material with an intrinsic thermal conductivity of κ_0, and the controllable heat sources can be described by matrix **Q**(**x**) with both coordinate and local power density distribution information. Without loss of generality, we assume a 1D system with n units and total length L. The heat conduction in the ATM is governed by

$$\frac{\partial}{\partial t}(\rho c T) = \nabla \cdot (\kappa_0 \nabla T) + \Phi, \qquad \text{(Equation 1)}$$

Please cite this article in press as: Wang et al., Macroscale anomalous heat conduction in active thermal metamaterials, Newton (2025), https://doi.org/10.1016/j.newton.2025.100255

where ρ and c are the density and thermal capacity, respectively; κ_0 is the intrinsic thermal conductivity; T is the temperature distribution; and Φ is the function of inner sources. To solve this equation, Green's function is introduced to calculate the temperature field induced by multiple sources and boundary conditions. The governing equations in the form of Green's function are as follows:

$$\frac{\rho c}{\kappa_0}\frac{\partial G(x,t,x',t')}{\partial t} = \frac{\partial^2 G(x,t,x',t')}{\partial x^2} + \frac{1}{\kappa_0}\sum_{i=1}^{n}\delta(x-x')\delta(t-t'), \quad \text{(Equation 2)}$$

where G is the Green's function of one point source, x' is the position of the source, t' is the time the source was applied, and δ is the unit-impulse function to describe the point source. Considering the 1D steady state, the temperature field of the ATM model can be calculated by Green's function as

$$T_{ATM}(x) = \frac{1}{\kappa_0}\sum_{i=1}^{n}\mathbf{Q}(x_i)\cdot G_i(x,x_i) + G_1(x)f_1 + G_2(x)f_2, \quad \text{(Equation 3)}$$

where x_i is the dimensionless position of each heat source within $[0, L]$ and $\mathbf{Q}(x_i)$ is the power density, $G_i(x, x_i)$ is the corresponding Green's function of each source, and $G_1(x)f_1$ and $G_2(x)f_2$ are the Green's function and temperature of two boundary conditions, respectively. According to the general solution of Green's function of the 1D steady-state point source, Green's function in our model is

$$G_i(x,x_i) = \left[H(x_i-x) - \frac{x_i}{L}\right](x-x_i) + \frac{x_i}{L}(L-x_i), \quad \text{(Equation 4)}$$

where $H(\cdot)$ is the Heaviside function.

To calculate the κ_{eff} of the ATM, we build an equivalent model, which is also a 1D medium but composed of different parts with different thermal conductivities without any heat sources (Figure 2A). Heat transfer in the equivalent model is governed by a heat conduction equation without the source terms: $\frac{\partial}{\partial\tau}(\rho cT) = \nabla\cdot(\kappa\nabla T)$

When we directly solve this equation under the 1D steady state, the temperature field is

$$T_{eq}(x) = \begin{cases} T_H - q\cdot\dfrac{x}{\kappa_1} & 0<x<x_1 \\ T_H - q\cdot\displaystyle\sum_{j=1}^{i-1}\frac{x_j-x_{j-1}}{\kappa_j} - q\cdot\frac{x-x_{i-1}}{\kappa_i} & x_{i-1}<x<x_i, 1<i\le n \end{cases}, \quad \text{(Equation 5)}$$

where q denotes the lumped heat flow as $q = (T_H - T_C)/\sum_{i=1}^{n}\frac{x_i-x_{i-1}}{\kappa_i}$ and κ_i denotes the thermal conductivity of unit i. Then, we make the ATM achieve the same temperature distribution as the equivalent model, which means that $[T_{ATM}(x) = T_{eq}(x)]$, and the heat flux through the medium at the inlet and outlet is equal ($Q_{in} = Q_{out}$), which implies that the sum of the internal source term intensities must be zero ($\sum q_i = 0$) and independent of the position of the sources. With the above two requirements, we solve a system of n equations:

$$\mathbf{T}_{\mathrm{ATM}}(\mathbf{x}) = \mathbf{T}_{\mathrm{eq}}(\mathbf{x}), \quad \text{(Equation 6)}$$

where $\mathbf{x} = [x_1, x_2, \ldots, x_{n-1}]$, and with $Q_{in} = Q_{out}$, we obtain the thermal conductivity matrix $\boldsymbol{\kappa} = [\kappa_1, \kappa_2, \ldots, \kappa_n]$. To verify the calculation method of the model, we do some numerical simulations as illustrated in Figure 2B. We set $\kappa_0 = 1\ \mathrm{W\cdot m^{-1}\cdot K^{-1}}$, $T_H = 328$ K, $T_C = 278$ K, $l_0 = 0.05$ m, and $L = 0.3$ m. It is seen that both temperature fields $T_{ATM}(x)$ and $T_{eq}(x)$ are piecewise and linearly distributed between every two adjacent boundaries, and the temperature distributions of the ATM and the equivalent model agree well.

Finally, we apply the equivalent medium theory (EMT) to calculate κ_{eff} by regarding the obtained ATM as a 1D series thermal resistance network as

$$\kappa_{eff} = \frac{L}{\displaystyle\sum_{i=1}^{n}\frac{x_i-x_{i-1}}{\kappa_i}}. \quad \text{(Equation 7)}$$

Using the above protocol, we design ATMs (i.e., $\mathbf{Q}(\mathbf{x})$) to achieve the same temperature field $T_{ATM}(x) = T_{eq}(x)$ with respect to the same boundary heat flux and obtain the corresponding κ_{eff}. ATMs enable the regulation of temperature fields and heat flux fields by modulating the heat source position and intensity specifically. This is crucial for the effective design and operation of ATMs, allowing for precise control and tuning of their thermal properties to achieve macroscale anomalous heat conduction.

Size-dependent κ_{eff}

First, we investigate how the internal heat sources affect κ_{eff}. The simplified model with pairs of heat and cold sources is depicted in Figure 3A, where a medium with an intrinsic thermal conductivity κ_0 and a total length L has two temperatures, T_H and T_C, on the left and right boundaries, respectively. The cold and heat sources with opposite power density, namely $-q_i$ and q_i, are set at x_i and $x_i + l_0$, such that $\sum q_i = 0$ is satisfied automatically regardless of the number and intensity of source pairs.

Then, we consider a medium containing N pairs of heat and cold sources where the distance of each pair is also set to l_0, which implies that the interval between each heat/cold source

Please cite this article in press as: Wang et al., Macroscale anomalous heat conduction in active thermal metamaterials, Newton (2025), https://doi.org/10.1016/j.newton.2025.100255

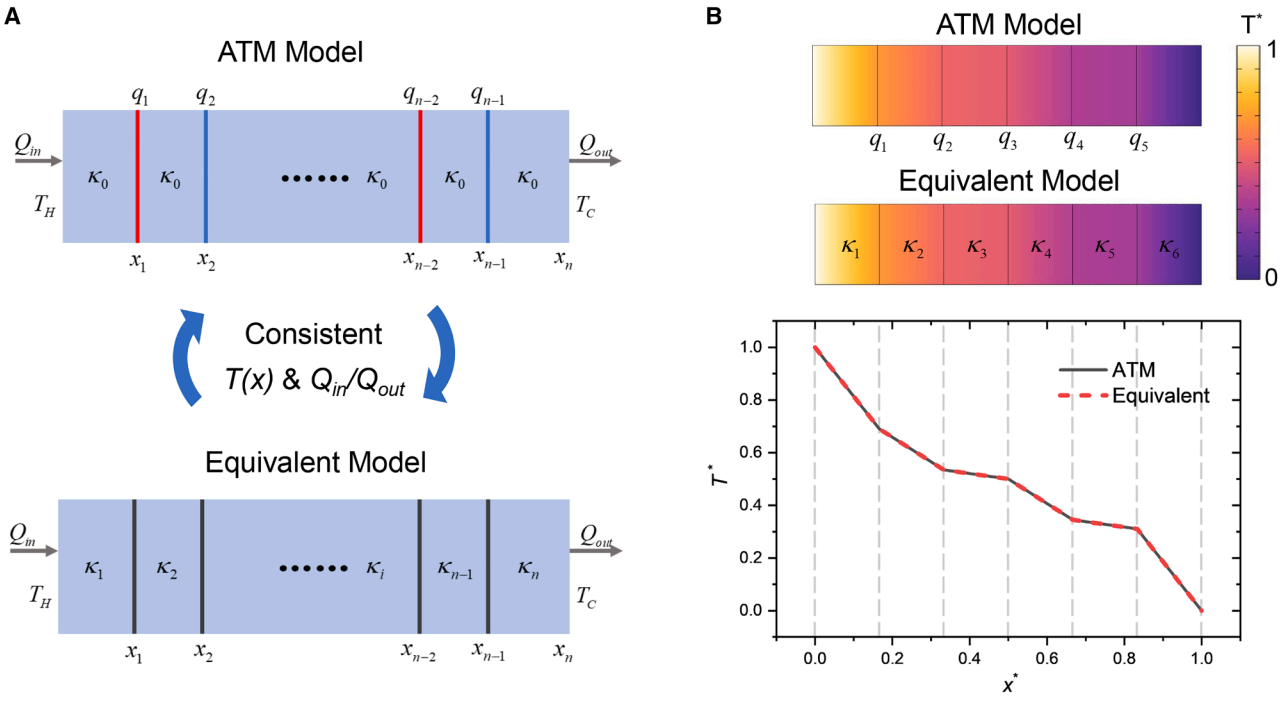

Figure 2. ATM model and equivalent model

(A) Schematic of ATM model and equivalent model. The ATM is composed of a base medium with an intrinsic thermal conductivity of κ_0 and multiple controllable internal heat sources. The controllable heat sources can be described by matrix q_i and x_i as coordinate and local power density distribution information. The equivalent model is a one-dimensional medium but composed of different parts with different thermal conductivities κ_i without any heat sources.

(B) Simulated temperature fields of two models. The ATM model consists of 5 inner sources, and the equivalent model consists of 6 parts with different thermal conductivity. The normalized temperature is $T^* = (T - T_C)/(T_H - T_C)$, and the normalized coordinate is $x^* = x/L$.

is l_0. At the same time, the source intensities q_i are kept consistent as q_0. Now, κ_{eff} is influenced by three factors: the source interval l_0, the ratio of L/l_0, and the source intensity q_0, as shown in Figure 3B. It is noted that the positive or negative value of q_0 represents the relationship between the order of the cold and hot sources and the direction of the external temperature gradient. If the hot source is followed by the cold source along the direction of the temperature gradient, then the source pair intensity is positive, and vice versa. When the source pair intensity q_0 is zero, κ_{eff} remains unchanged

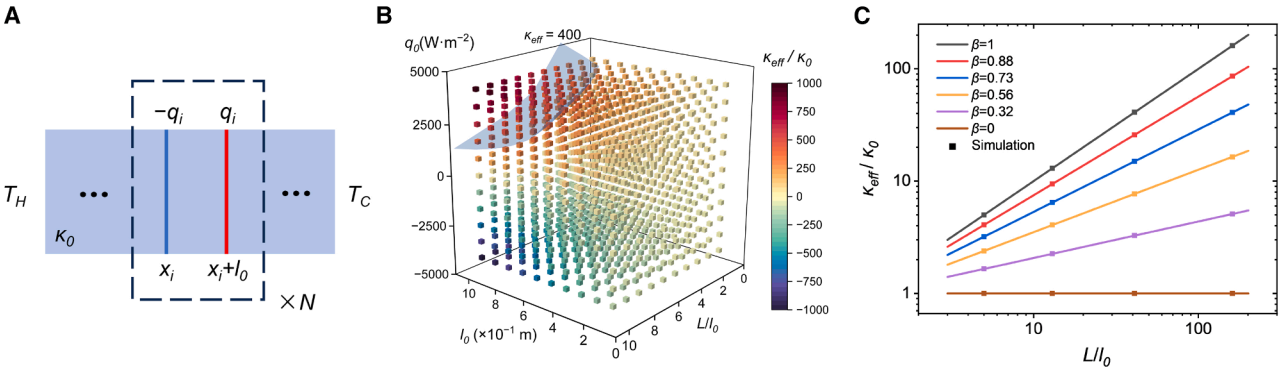

Figure 3. Schematic of ATMs and k_{eff}

(A) Schematic of ATMs with multiple heat source pairs. The ATM composed of a medium with an intrinsic thermal conductivity κ_0 and a total length L has two temperatures, T_H and T_C, on the left and right boundaries. The cold and heat sources with opposite power density, namely, $-q_i$ and q_i, are set at x_i and $x_i + l_0$.

(B) Changes in κ_{eff} of the multiple pairs ATMs. The color represents the magnitude of κ_{eff}/κ_0 ($\kappa_0 = 1\ W{\cdot}m^{-1}{\cdot}K^{-1}$). The light blue surface represents that the κ_{eff} is equal to that of copper ($400\ W{\cdot}m^{-1}{\cdot}K^{-1}$). The coordinates of the three directions are the source interval l_0, the ratio of L/l_0, and the source intensity q_0, respectively.

(C) Normalized thermal conductivity versus normalized length of modulated ATMs. Different curves represent the κ_{eff}-L relationship ($0 \le \beta \le 1$) under different source modulation parameters.

Please cite this article in press as: Wang et al., Macroscale anomalous heat conduction in active thermal metamaterials, Newton (2025), https://doi.org/10.1016/j.newton.2025.100255

regardless of l_0 and L/l_0. When the source pair intensity is positive, κ_{eff} increases with the increase in the absolute value of q_0, l_0, and L/l_0, respectively. If we keep q_0 and l_0 constant, the size-dependent κ_{eff} emerges; that is, κ_{eff} changes positively with L. At the same time, when l_0 is negative, κ_{eff} decreases with the increase in the absolute value of q_0, l_0, and L/l_0, respectively. Also, κ_{eff} changes inversely with L if q_0 and l_0 are constant. It can be observed that the positive or negative value of the intensity, that is, the order of cold and hot sources, is the factor that determines the κ_{eff}. It is worth noting that by taking advantage of this size effect, we can modulate the κ_{eff} of the ATM to exceed that of common high thermal conductivity materials (such as copper, indicated by the light blue surface in Figure 3B), thereby greatly expanding the manipulation capabilities and thermal conductivity limit of thermal metamaterials.

To investigate the anomalous size-dependent relationship of κ_{eff}, we keep the interval between each source $l_0 = 0.05$ m and modulate the power density of heat sources $\mathbf{Q}(\mathbf{x})$ to find the relationship $\kappa_{eff} = cL^{\beta}$. We use the following equation to describe the intensity of the internal heat/cold sources:

$$\begin{cases} \mathbf{Q}[x = (2i - 1)\cdot l_0] = -q_i = -q_0\cdot i^{\alpha} \\ \mathbf{Q}[x = (2i)\cdot l_0] = q_i = q_0\cdot i^{\alpha} \end{cases}, \qquad \text{(Equation 8)}$$

where i is the number of the source pair, q_i is the power density of the ith source pair, q_0 is the basic power density, and α is the modulation coefficient. For each value of q_0, we find the optimal value of parameter α as $\alpha* = \arg\min_{\alpha\in[-1,0]}\left(\min_{\beta,c}\sum_{L_N}[\kappa_{eff}(\alpha,L_N) - c(\alpha)L_N{}^{\beta(\alpha)}]^2\right)$, where $L_N = (2N + 1)*l_0$, $N = 1,2,3\ldots$ (see Note S1 for detailed steps and parameters). Figure 3C plots some typical κ_{eff}-L relationship curves under different $\mathbf{Q}(\mathbf{x})$. It can be clearly seen that κ_{eff} shows a good logarithmic relationship with the system size. When $\mathbf{Q}(\mathbf{x}) = 0$, there are no sources inside the ATMs, and conventional purely diffusive heat conduction occurs, corresponding to the size-independent κ_{eff} and $\beta = 0$. In contrast, when $\mathbf{Q}(\mathbf{x}) \neq 0$, κ_{eff} becomes size dependent, and the macroscale anomalous heat conduction occurs, corresponding to $\beta \neq 0$. This size-dependent anomalous heat conduction successfully mimics different heat conduction states in the microscale. $\beta = 1$ corresponds to ballistic-analog heat conduction, and $0 < \beta < 1$ corresponds to ballistic-diffusive-analog heat conduction, which is an intermediate state between ballistic and diffusive heat conduction. Further, we simulate six different heat conduction states with different β. We set $T_H = 328$ K, $T_C = 278$ K, $l_0 = 0.05$ m, and $\kappa_0 = 1$ W·m^{-1}·K^{-1}. The left and right sides are kept at constant temperature boundary conditions, while the top and bottom sides are insulated. The κ_{eff} in different states are shown as data points in Figure 3C, and the corresponding normalized temperature curves, under two lengths, $L_1/l_0 = 13$ and $L_2/l_0 = 41$, with different numbers of source pairs, are shown in Figure 4A. It is seen that the temperature curves fluctuate along with the distributions of heat and cold sources, and with the decrease of β from 1 to 0, the temperature fluctuations are gradually weakened and tend to approach the temperature gradient with $\beta = 0$. The number of source pairs merely increases the frequency of temperature fluctuations but does not influence the main temperature trend. When $\beta = 1$ (at the ballistic-analog regime), the temperature fluctuates like wave propagation. When $\beta = 0$ (at the diffusive regime), the temperature curve is linear, aligning with the temperature gradient without temperature fluctuations. When $0 < \beta < 1$ (ballistic-diffusive-analog regime), the temperature curves along the coordinates increase first and then decrease gradually, transiting from fluctuation to diffusion along with the temperature gradient. By comparing L_1 and L_2 under each anomalous heat conduction state, it is revealed that larger system size and more source pairs correspond to larger excess temperature over the maximum temperature applied externally. Figure 4B illustrates the normalized temperature fields of the case when $L_2/l_0 = 41$, offering a vivid illustration of the macroscale anomalous heat conduction phenomenon with exponent coefficient β from 1 to 0.

To elucidate the underlying mechanism of macroscale anomalous heat conduction, we theoretically analyze the internal temperature gradient distribution of ATMs under different heat conduction states (β). Due to the continuous fluctuation of temperature between the cold and hot sources, the direction of the temperature gradient, i.e., the sign of dT/dx, is constantly changing. Thus, the temperature gradients in both directions are plotted separately. The positive temperature gradients are shown in Figure 4C, while the negative temperature gradients are shown in Figure 4D. It is observable that when $\beta = 1$, both the positive and negative temperature gradients remain unchanged and have the same magnitude (red dots). When $\beta = 0$, the temperature gradient always maintains a fixed value of $(T_H - T_C)/L$, without any direction change (gray dotted line). While $0 < \beta < 1$, the positive and negative temperature gradients exhibit completely different trends. The positive temperature gradient gradually decreases along the direction of heat transfer, whereas the negative temperature gradient sustains a constant value. The reasons can be explained as follows. The defining trait of diffusive conduction is that the flux is proportional to the temperature gradient ($q \propto dT/dx$). The ATMs reconfigure the internal temperature field, allowing heat to be transferred within the medium without attenuation directly from the hot side to the cold side, breaking the conventional size-independent Fourier's laws. The ATMs make the heat flux proportional to the temperature difference rather than the temperature gradient, exhibiting a similar key feature of the ballistic heat conduction that occurred in microscale. At this point, changes in system size will no longer affect the heat flux (Note S2; Figure S1). The intermediate state ($0 < \beta < 1$) combines the characteristics of both, but the reconstructive temperature field of ATMs is not sufficient to maintain the constant heat flux, leading to the continuous decrease of the positive temperature gradient along the direction of heat transfer until it approaches purely diffusive heat conduction.

Finally, we set up experiments to verify the anomalous heat conduction phenomenon in ATMs. The schematic diagram of the experimental setup is shown in Figure 5A. Four pairs of Peltier modules are embedded in the base medium for alternative heating or cooling with an interval of 0.05 m to fabricate the ATM. The heating and cooling powers $\mathbf{Q}(\mathbf{x})$ in the experiments are quantified by theoretical analysis and adjusted by the power controller. Since the widths of the Peltier modules and the base

Please cite this article in press as: Wang et al., Macroscale anomalous heat conduction in active thermal metamaterials, Newton (2025), https://doi.org/10.1016/j.newton.2025.100255

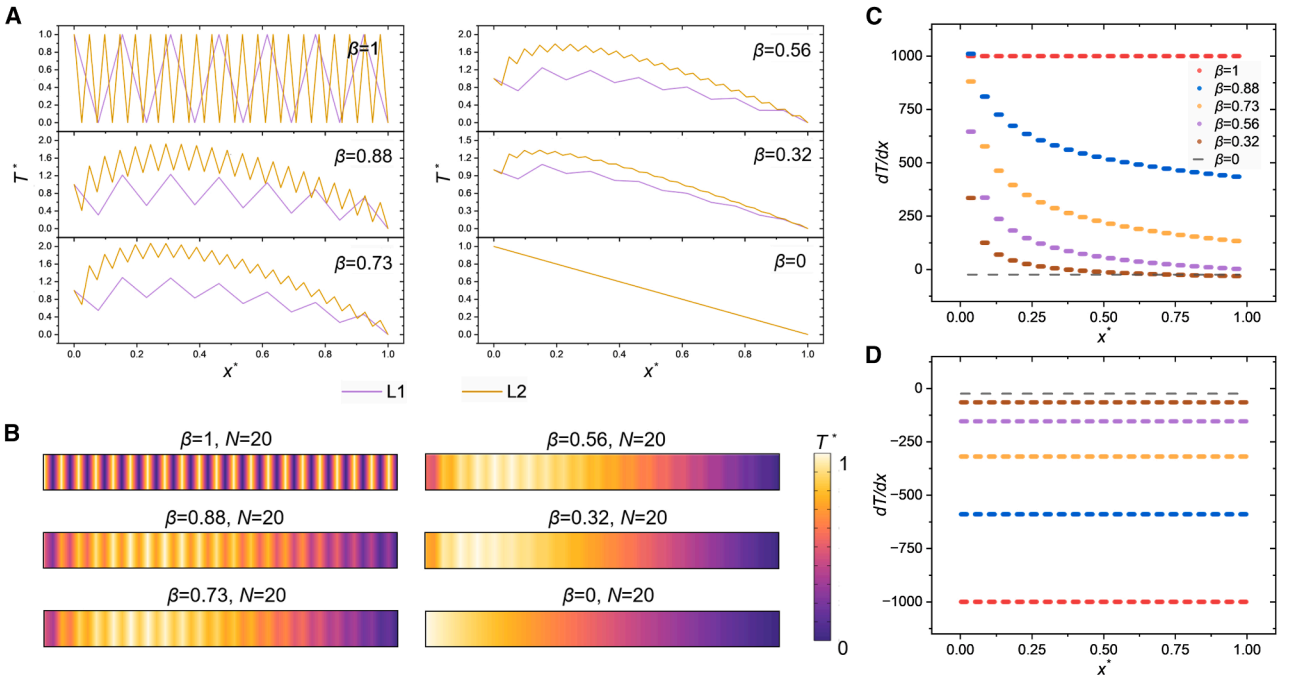

Figure 4. Macroscale anomalous heat conduction phenomenon in ATMs

(A) Normalized temperature of ATMs under different macroscale anomalous heat conduction. The normalized temperature is $T^* = (T - T_C)/(T_H - T_C)$, and the normalized coordinate is $x^* = x/L$. Two colored curves represent the cases under two lengths, $L_1/l_0 = 13$ and $L_2/l_0 = 41$, with different numbers of source pairs, respectively.

(B) Temperature distribution of ATMs under different macroscale anomalous heat conduction of the case where $L_2/l_0 = 41$ ($N = 20$). The color bar represents the normalized temperature.

(C and D) Positive temperature gradient (C) and negative temperature gradient (D) of ATMs under different anomalous heat conduction. The temperature gradients under different states are distinguished by different colored dots with β from 0 to 1.

medium are kept the same, the heat conduction along the base medium can be considered as quasi-1D. The temperature fields measured by the infrared (IR) camera and the corresponding temperature curves along the red dashed center line are shown in Figures 5B–5E. With different **Q**(**x**), different temperature fields can be achieved, corresponding to different heat conduction states with $\beta = 1$ (Figure 5B), $\beta = 0.88$ (Figure 5C), $\beta = 0.56$ (Figure 5D), and $\beta = 0$ (Figure 5E) regimes (see detailed experimental settings in Note S1 and Table S2). It can be observed that the experimental temperature curves are close to those in simulations, verifying the macroscale anomalous heat conduction phenomenon with varying β. The deviation between experiments and simulations arises from two aspects: one is non-ideal point heat or cold sources due to the certain width of each Peltier module and the other is the remaining air convection effect in the experiments.

DISCUSSION

In summary, we achieve and demonstrate macroscale anomalous heat conduction featuring size effects in ATMs, replicating microscale transport phenomena across ballistic, ballistic-diffusive, and diffusive regimes. By modulating internal cold and heat sources, ATMs reconstruct temperature fields and introduce a new degree of freedom to control size-dependent κ_{eff}. Our theoretical analysis, simulations, and experiments reveal κ_{eff} scaling with exponent β from 1 to 0. This work not only suggests a distinct mechanism to achieve anomalous heat conduction by ATMs but also broadens the design potential of thermal metamaterials, with future work extending to higher dimensions, complex boundaries, and transient processes.

METHODS

Numerical simulations

Numerical simulations of the temperature field and heat flux in ATMs are conducted using the finite-element method with COMSOL Multiphysics 6.1. For the 2D model of ATMs, the left and right boundaries are set as constant temperature boundary conditions, and the top and bottom boundaries are set as periodic boundary conditions.

Experimental setup

In the experiment, the base medium of the ATM is polytetrafluoroethylene ($\kappa_0 = 0.25$ W·m^{-1}·K^{-1}) with dimensions of 450 × 23 × 5 mm^3. Four pairs of Peltier modules (TECooler, HT016071) with a uniform size of 23 × 6 mm^2 are embedded in it. The left and right boundaries of the ATM are kept at T_H = 328 K and T_C = 278 K, respectively, with a water bath, and the other boundaries are insulated with porous foam plastics.

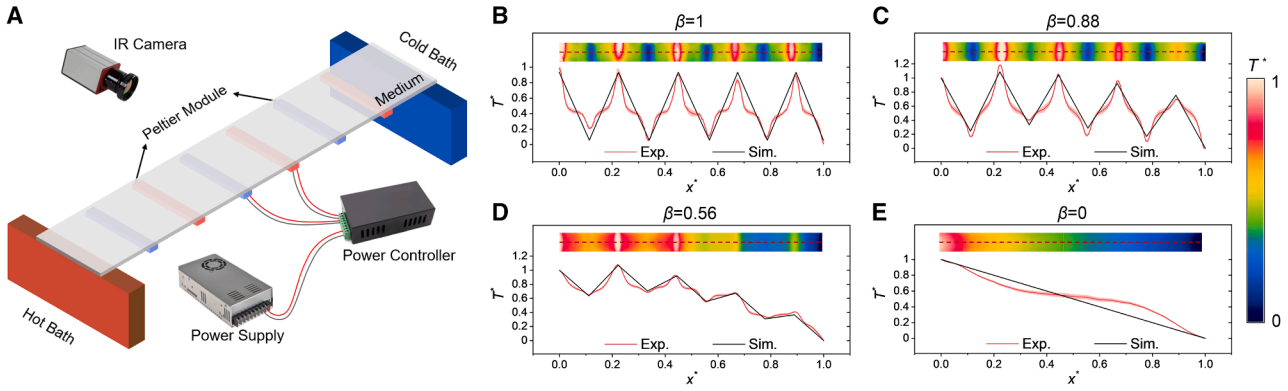

Figure 5. Experimental observation of anomalous heat conduction

(A) Schematic diagram of the experimental setup. Four pairs of Peltier modules are embedded in the base medium for alternative heating or cooling to fabricate the ATM. The temperature boundary conductions are kept with hot and cold baths. The heating and cooling powers are adjusted by the power controller and power supply. The temperature fields are measured by the IR camera.

(B–E) Temperature curve and temperature distribution of the ATMs in IR camera under different anomalous heat conduction states: $\beta = 1$ (B), $\beta = 0.88$ (C), $\beta = 0.56$ (D), and $\beta = 0$ (E), respectively. The color bar represents the temperature distribution, and the curves represent the temperature along the red dotted center line. The light red shadow surrounding the red curve represents experimental error. The normalized temperature is $T^* = (T - T_C)/(T_H - T_C)$, and the normalized coordinate is $x^* = x/L$.

The temperature fields are measured by the IR camera (SC620, FLIR).

RESOURCE AVAILABILITY

Lead contact

Requests for further information and resources should be directed to and will be fulfilled by the lead contact, Run Hu (hurun@hust.edu.cn).

Materials availability

This study did not generate new unique reagents.

Data and code availability

- All data reported in this paper will be shared by the lead contact upon request.
- This paper does not report original code.
- Any additional information required to reanalyze the data reported in this paper is available from the lead contact upon request.

ACKNOWLEDGMENTS

R.H. acknowledges financial support from the National Natural Science Foundation of China (52422603, 92463311, 52161160332, and 52411540235), the Science and Technology Program of Hubei Province (2023AFA072), the Interdisciplinary Research Program of HUST (5003120094), the Open Research Fund of Suzhou Laboratory (SZLAB-1508-2024-TS016), and the Shenzhen Technology Project (JCYJ20241202123700001).

AUTHOR CONTRIBUTIONS

Conceptualization, Zhaochen Wang, X.Q., X.L., and R.H.; methodology, Zhaochen Wang and Q.L.; investigation, Zhaochen Wang and Q.L.; writing – original draft, Zhaochen Wang; writing – review & editing, R.H.; data curation, Q.L.; validation, L.X., W.K., Y.Y., and X.L.; discussion, L.X.; supervision, Zhiqiang Wang, X.Q., and R.H.; funding acquisition, R.H.

DECLARATION OF INTERESTS

The authors declare no competing interests.

SUPPLEMENTAL INFORMATION

Supplemental information can be found online at https://doi.org/10.1016/j.newton.2025.100255.

Received: April 25, 2025
Revised: July 11, 2025
Accepted: September 5, 2025

REFERENCES

1. Fermi, E., Pasta, P., Ulam, S., and Tsingou, M. (1955). Studies of the Nonlinear Problems. Los Alamos National Laboratory, Los Alamos, NM, Report No. LA-1940. https://doi.org/10.2172/4376203.
2. Wu, G., and Dong, J. (2005). Anomalous heat conduction in a carbon nanowire: Molecular dynamics calculations. Phys. Rev. B *71*, 115410. https://doi.org/10.1103/PhysRevB.71.115410.
3. Yang, N., Zhang, G., and Li, B. (2010). Violation of Fourier's law and anomalous heat diffusion in silicon nanowires. Nano Today *5*, 85–90. https://doi.org/10.1016/j.nantod.2010.02.002.
4. Henry, A., and Chen, G. (2009). Anomalous heat conduction in polyethylene chains: Theory and molecular dynamics simulations. Phys. Rev. B *79*, 144305. https://doi.org/10.1103/PhysRevB.79.144305.
5. Yang, L., Tao, Y., Zhu, Y., Akter, M., Wang, K., Pan, Z., Zhao, Y., Zhang, Q., Xu, Y.-Q., Chen, R., et al. (2021). Observation of superdiffusive phonon transport in aligned atomic chains. Nat. Nanotechnol. *16*, 764–768. https://doi.org/10.1038/s41565-021-00884-6.
6. Ni, X., Leek, M.L., Wang, J.-S., Feng, Y.P., and Li, B. (2011). Anomalous thermal transport in disordered harmonic chains and carbon nanotubes. Phys. Rev. B *83*, 045408. https://doi.org/10.1103/PhysRevB.83.045408.
7. Ray, U., and Limmer, D.T. (2019). Heat current fluctuations and anomalous transport in low-dimensional carbon lattices. Phys. Rev. B *100*, 241409. https://doi.org/10.1103/PhysRevB.100.241409.
8. Chien, H.-C., Peng, W.-T., Chiu, T.-H., Wu, P.-H., Liu, Y.-J., Tu, C.-W., Wang, C.-L., and Lu, M.-C. (2020). Heat Transfer of Semicrystalline Nylon Nanofibers. ACS Nano *14*, 2939–2946. https://doi.org/10.1021/acsnano.9b07493.

9. Yoon, M., Howe, J., Tibbetts, G., Eres, G., and Zhang, Z. (2007). Polygonization and anomalous graphene interlayer spacing of multi-walled carbon nanofibers. Phys. Rev. B *75*, 165402. https://doi.org/10.1103/PhysRevB.75.165402.

10. Hu, B., Yang, L., and Zhang, Y. (2006). Asymmetric Heat Conduction in Nonlinear Lattices. Phys. Rev. Lett. *97*, 124302. https://doi.org/10.1103/PhysRevLett.97.124302.

11. Wang, J., Liu, T.X., Luo, X.Z., Xu, X.-L., and Li, N. (2020). Anomalous energy diffusion in two-dimensional nonlinear lattices. Phys. Rev. E *101*, 012126. https://doi.org/10.1103/PhysRevE.101.012126.

12. Wang, L., Wu, Z., and Xu, L. (2015). Super heat diffusion in one-dimensional momentum-conserving nonlinear lattices. Phys. Rev. E *91*, 062130. https://doi.org/10.1103/PhysRevE.91.062130.

13. Narayan, O., and Ramaswamy, S. (2002). Anomalous Heat Conduction in One-Dimensional Momentum-Conserving Systems. Phys. Rev. Lett. *89*, 200601. https://doi.org/10.1103/PhysRevLett.89.200601.

14. Feng, T., He, J., Rai, A., Hun, D., Liu, J., and Shrestha, S.S. (2020). Size Effects in the Thermal Conductivity of Amorphous Polymers. Phys. Rev. Applied *14*, 044023. https://doi.org/10.1103/PhysRevApplied.14.044023.

15. Zhang, Z., Ouyang, Y., Cheng, Y., Chen, J., Li, N., and Zhang, G. (2020). Size-dependent phononic thermal transport in low-dimensional nanomaterials. Phys. Rep. *860*, 1–26. https://doi.org/10.1016/j.physrep.2020.03.001.

16. Li, B., and Wang, J. (2003). Anomalous Heat Conduction and Anomalous Diffusion in One-Dimensional Systems. Phys. Rev. Lett. *91*, 044301. https://doi.org/10.1103/PhysRevLett.91.044301.

17. Liu, S., Hänggi, P., Li, N., Ren, J., and Li, B. (2014). Anomalous Heat Diffusion. Phys. Rev. Lett. *112*, 040601. https://doi.org/10.1103/PhysRevLett.112.040601.

18. Chen, G. (2021). Non-Fourier phonon heat conduction at the microscale and nanoscale. Nat. Rev. Phys. *3*, 555–569. https://doi.org/10.1038/s42254-021-00334-1.

19. Ding, Z., Zhou, J., Song, B., Chiloyan, V., Li, M., Liu, T.-H., and Chen, G. (2018). Phonon Hydrodynamic Heat Conduction and Knudsen Minimum in Graphite. Nano Lett. *18*, 638–649. https://doi.org/10.1021/acs.nanolett.7b04932.

20. Juntunen, T., Vänskä, O., and Tittonen, I. (2019). Anderson Localization Quenches Thermal Transport in Aperiodic Superlattices. Phys. Rev. Lett. *122*, 105901. https://doi.org/10.1103/PhysRevLett.122.105901.

21. Rego, L.G.C., and Kirczenow, G. (1998). Quantized thermal conductance of dielectric quantum wires. Phys. Rev. Lett. *81*, 232–235. https://doi.org/10.1103/PhysRevLett.81.232.

22. Luckyanova, M.N., Garg, J., Esfarjani, K., Jandl, A., Bulsara, M.T., Schmidt, A.J., Minnich, A.J., Chen, S., Dresselhaus, M.S., Ren, Z., et al. (2012). Coherent Phonon Heat Conduction in Superlattices. Science *338*, 936–939. https://doi.org/10.1126/science.1225549.

23. Liu, Z., Cao, P.-C., Xu, L., Xu, G., Li, Y., and Huang, J. (2024). Higher-Order Topological In-Bulk Corner State in Pure Diffusion Systems. Phys. Rev. Lett. *132*, 176302. https://doi.org/10.1103/PhysRevLett.132.176302.

24. Ju, R., Cao, P.C., Wang, D., Qi, M., Xu, L., Yang, S., Qiu, C.W., Chen, H., and Li, Y. (2024). Nonreciprocal Heat Circulation Metadevices. Adv. Mater. *36*, 2309835. https://doi.org/10.1002/adma.202309835.

25. Xu, G., Zhou, X., Yang, S., Wu, J., and Qiu, C.-W. (2023). Observation of bulk quadrupole in topological heat transport. Nat. Commun. *14*, 3252. https://doi.org/10.1038/s41467-023-39117-w.

26. Wang, Z., Liu, T., Zhu, Z., Luo, X., and Hu, R. (2024). Periodicity alters topological states in thermal diffusion system. Int. J. Heat Mass Transf. *235*, 126182. https://doi.org/10.1016/j.ijheatmasstransfer.2024.126182.

27. Hu, R., Xi, W., Liu, Y., Tang, K., Song, J., Luo, X., Wu, J., and Qiu, C.-W. (2021). Thermal camouflaging metamaterials. Mater. Today *45*, 120–141. https://doi.org/10.1016/j.mattod.2020.11.013.

28. Hu, R., Liu, Y., Shin, S., Huang, S., Ren, X., Shu, W., Cheng, J., Tao, G., Xu, W., Chen, R., and Luo, X. (2020). Emerging Materials and Strategies for Personal Thermal Management. Adv. Energy Mater. *10*, 1903921. https://doi.org/10.1002/aenm.201903921.

29. Zhu, Z., Wang, Z., Liu, T., Luo, X., Qiu, C., and Hu, R. (2023). Field-coupling topology design of general transformation multiphysics metamaterials with different functions and arbitrary shapes. Cell Rep. Phys. Sci. *4*, 101540. https://doi.org/10.1016/j.xcrp.2023.101540.

30. Zhu, Z., Wang, Z., Liu, T., Xie, B., Luo, X., Choi, W., and Hu, R. (2024). Arbitrary-shape transformation multiphysics cloak by topology optimization. Int. J. Heat Mass Transf. *222*, 125205. https://doi.org/10.1016/j.ijheatmasstransfer.2024.125205.

31. Yang, F., Zhang, Z., Xu, L., Liu, Z., Jin, P., Zhuang, P., Lei, M., Liu, J., Jiang, J.-H., Ouyang, X., et al. (2024). Controlling mass and energy diffusion with metamaterials. Rev. Mod. Phys. *96*, 015002. https://doi.org/10.1103/RevModPhys.96.015002.

32. Wang, Z., Zhu, Z., Liu, T., and Hu, R. (2022). Inverse design of thermal metamaterials with holey engineering strategy. J. Appl. Phys. *132*, 145102. https://doi.org/10.1063/5.0108743.

33. Zhang, Z., Xu, L., Qu, T., Lei, M., Lin, Z.-K., Ouyang, X., Jiang, J.-H., and Huang, J. (2023). Diffusion metamaterials. Nat. Rev. Phys. *5*, 218–235. https://doi.org/10.1038/s42254-023-00565-4.

34. Li, Y., Li, W., Han, T., Zheng, X., Li, J., Li, B., Fan, S., and Qiu, C.-W. (2021). Transforming heat transfer with thermal metamaterials and devices. Nat. Rev. Mater. *6*, 488–507. https://doi.org/10.1038/s41578-021-00283-2.

35. Sha, W., Xiao, M., Zhang, J., Ren, X., Zhu, Z., Zhang, Y., Xu, G., Li, H., Liu, X., Chen, X., et al. (2021). Robustly printable freeform thermal metamaterials. Nat. Commun. *12*, 7228. https://doi.org/10.1038/s41467-021-27543-7.

36. Wu, Y.-F., Wang, B., Wu, C.-L., Yao, N.-Z., Wang, H., Wang, X., and Wang, X. (2025). Active thermal cloaks enabled by active coordinate transformation theory. Int. Commun. Heat Mass Transf. *164*, 108798. https://doi.org/10.1016/j.icheatmasstransfer.2025.108798.

37. Guo, J., and Qu, Z.G. (2018). Thermal cloak with adaptive heat source to proactively manipulate temperature field in heat conduction process. Int. J. Heat Mass Transf. *127*, 1212–1222. https://doi.org/10.1016/j.ijheatmasstransfer.2018.07.035.

38. Xu, L.J., Yang, S., and Huang, J.P. (2020). Effectively infinite thermal conductivity and zero-index thermal cloak. EPL *131*, 24002. https://doi.org/10.1209/0295-5075/131/24002.

39. Li, Y., Zhu, K.-J., Peng, Y.-G., Li, W., Yang, T., Xu, H.-X., Chen, H., Zhu, X.-F., Fan, S., and Qiu, C.-W. (2019). Thermal meta-device in analogue of zero-index photonics. Nat. Mater. *18*, 48–54. https://doi.org/10.1038/s41563-018-0239-6.

40. Guo, J., Xu, G., Tian, D., Qu, Z., and Qiu, C.W. (2022). Passive Ultra-Conductive Thermal Metamaterials. Adv. Mater. *34*, 2200329. https://doi.org/10.1002/adma.202200329.

41. Xu, L., Yang, S., and Huang, J. (2019). Dipole-assisted thermotics: Experimental demonstration of dipole-driven thermal invisibility. Phys. Rev. E *100*, 062108. https://doi.org/10.1103/PhysRevE.100.062108.